Chapter 6
Refractory Oxides

Jeffrey D. Smith and William G. Fahrenholtz

Abstract Refractory oxides encompass a broad range of unary, binary, and ternary ceramic compounds that can be used in structural, insulating, and other applications. The chemical bonds that provide cohesive energy to the crystalline solids also influence properties such as thermal expansion coefficient, thermal conductivity, elastic modulus, and heat capacity. This chapter provides a historical perspective on the use of refractory oxide materials, reviews applications for refractory oxides, overviews fundamental structure–property relations, describes typical processing routes, and summarizes the properties of these materials.

1 Introduction

The term *refractory* refers to materials that are resistant to the effects of heat. Refractory oxides, therefore, are ceramic materials that can be used at elevated temperatures. These nondescript restrictions allow nearly any oxide to be classified as refractory. For this article, refractory oxides will refer, somewhat arbitrarily, to common crystalline compounds with melting temperatures of at least 1,800°C. These compounds can contain one or more metal or metalloid cations bonded to oxygen. As an introduction to the topic, this section provides a brief historic overview of materials commonly used in the refractories industry, including some lower melting temperature materials. The section also reviews some current trends in the industries that produce and use refractory oxides. The other sections of this chapter focus on phase-pure oxide ceramics that can be used at elevated temperatures.

Historically, most of the oxides that were used in refractory applications were traditional ceramics prepared from clays or other readily available mineral-based raw materials. The major categories of traditional refractories are fire clays, high aluminas, and silica [1]. The choice of material for traditional refractory applications, as with advanced material applications, was and is based on balancing cost and performance/lifetime. The ultimate use temperatures and applications for some common refractories are summarized in Table 1 [2, 3]. The production, properties, and uses of some of these materials are discussed in more detail in the other chapters

J.F. Shackelford and R.H. Doremus (eds.), *Ceramic and Glass Materials: Structure, Properties and Processing*.

Table 1 Compositions, ultimate use temperatures, and applications for some common traditional refractory materials

Class	Material	Phases	Use Temp (°C)	Applications
Fire clay	Low heat duty	Mullite, glass, quartz	Up to 1500	Kiln linings
	High heat duty	Mullite, glass		Crucibles
High alumina	Kyanite	α-Al_2O_3, mullite, glass	Up to 1800	Metal handling
				Lab ware
Silica	Silica	Tridymite, cristobalite	1650	Glass tanks crowns

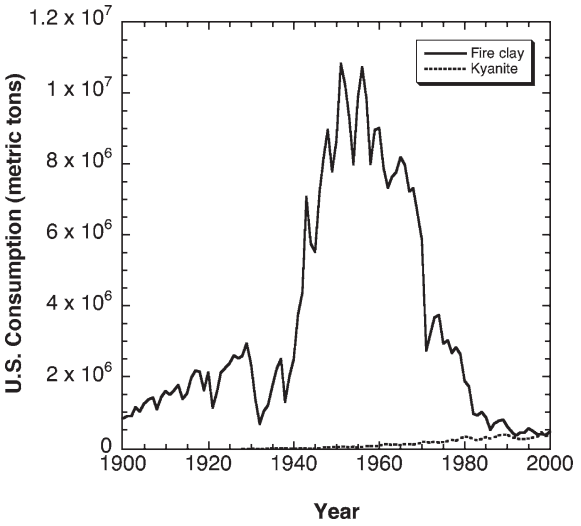

Fig. 1 Historic production numbers for fireclay and high alumina (labeled kyanite) brick

of this volume. A brief overview of fireclays, high aluminas, and silica is provided here followed by a description of the evolution of the refractories industry.

Although no strict geologic definition exists [4], fireclays can be defined as clay minerals that have pyrometric cone equivalent (PCE) values of 19 or greater following ASTM specification C24–01 (Standard Test Method for Pyrometric Cone Equivalent (PCE) of Fireclay and High Alumina Refractory Materials) [5]. Most refractory products are fabricated from what are considered high heat duty fire clays, which have a PCE value of 27 or higher (~1600°C). Fireclays have Al_2O_3 contents that range from 20 to 45 wt%, with silica being the other major constituent [6]. Because of their ease of fabrication, resistance to chemical attack, and low cost, fireclay bricks are still widely used as refractory materials. Applications for fireclay refractory brick include insulation behind hot-face materials, furnace linings, and specialty applications such as laboratory crucibles and setters. Historic consumption of fireclay was significantly greater when fireclay refractory brick demand from the U.S. steel industry was at its peak of ~10,000,000 metric tons in the early 1950s (Fig. 1). The decline in demand from the steel industry was due to changes that included higher use temperatures and a shift to

basic practices to improve steel cleanliness. The changing process requirements spurred the development of advanced refractory ceramics such as high alumina castables and basic brick, both of which are prepared from highly beneficiated oxides rather than unrefined minerals. In the past quarter century, fireclay refractories have evolved from a state-of-the-art engineered material to a commodity item that often originates from countries having low labor costs.

Most high alumina refractories are clay-based ceramics to which an alumina-rich mineral is added to chemically react with a majority of the silica present to promote mullite formation [7]. High alumina refractories contain a minimum of 60 wt% Al_2O_3, although the Al_2O_3 content can be >99% for specialty products. High alumina refractories can be produced from fire clays used in combination with alumina-rich minerals such as diaspore or bauxite [8]. Reduction of the amount of free silica (consumed in the formation of mullite) results in increased use temperature for high alumina refractories compared with fire clay refractories, up to 1800°C for some materials. The greater mullite content of high aluminas gives them improved creep resistance and better corrosion behavior. High alumina refractories were developed for steel industry applications that were beyond the performance limits of fireclay refractories. High alumina bricks continue to find use in a wide range of industrial applications including aluminum melting and incineration. Today, use of high alumina materials is approximately equivalent to fireclays (Fig. 1).

Silica refractories can be crystalline or amorphous (fused). Most silica refractories are produced from silica-rich minerals such as quartz and flint and have SiO_2 contents of 98 wt% or higher. For crystalline refractories, a mineralizer-like CaO is added to promote crystallization to cristobalite and/or tridymite thereby eliminating the displacive-phase transformation associated with the α to β quartz transition at 573°C. Displacive transformations are typically associated with substantial volume changes that can be quite destructive. Because of the relatively low theoretical density of silica (~2.3 g cm^{-3} for cristobalite and tridymite), silica bricks are often used to construct arched furnace crowns [8]. Unlike most ceramic materials, silica bricks are resistant to creep at elevated temperature allowing them to be used for extended durations at temperatures approaching the melting temperature. Thus, even though silica melts below the 1800°C limit considered in this article, it has been included because of its high use temperature. The recent trend in the glass industry to convert to oxy-fuel firing has decreased the usage of silica brick because higher temperatures and water vapor concentration in oxy-fuel fired glass hearths promotes alkali-induced corrosion of silica.

In the middle part of the twentieth century, the ceramics industry began a general shift from traditional ceramics toward more advanced (highly engineered) materials. Traditional ceramics are derived from minerals and can have significant variations in composition and performance depending upon the source of the raw material. Traditional ceramics also tend to contain significant amounts of glassy phases or impurities. In contrast, advanced ceramics are usually phase pure oxides that are derived from high-purity industrial chemicals. Advanced ceramics can be single phase or multiphase, but they are essentially phase pure meaning that they contain no significant (0.5 wt% or less) glassy phase or impurities. The cost of advanced ceramics compared with traditional materials created the need for application-specific compositions. Thus, advanced materials are implemented specifically where they are needed to optimize system performance. The selection of advanced materials is still driven by the performance-cost balance. Understanding materials performance and selecting the

proper material for a particular application requires knowledge of material properties such as those discussed later in this chapter.

Even though many refractory oxides are engineered to optimize performance in a single application, any number of ceramics can be selected for a particular application. Examples of some of the oxides that can be used at high temperatures, along with their melting temperatures, are listed in Tables 2–5 for oxides containing one, two, or more cations [9–11]. It should be noted that consensus on the melting temperature of specific oxides is tenuous, so values should be considered as approximations; this is especially true in the case of oxides having melting temperatures well above 2000°C. These lists are not intended to be comprehensive (although Tables 2 and 5 contain all of the unary and ternary refractory oxides that the authors could identify), but the lists are long enough to emphasize that a large number of candidates exist for any application. Tables 3 and 4 are samplings from the hundreds of two component refractory oxides that are available.

From the larger list of binary refractory oxides, aluminate compounds are listed in Table 3 to emphasize that a family of materials that contain one compound with a high melting temperature will tend to form other compounds with high melting temperatures. Within the aluminate family, a number of compounds are formed that might not

Table 2 Melting temperatures of refractory oxides containing a single cation

Oxide	T_m (°C)
Al_2O_3	2020
BaO	1925
BeO	2570
CaO	2600
CeO_2	2600
Cr_2O_3	2400
CuO	1800
Eu_2O_3	2240
Gd_2O_3	2350
HfO_2	2780
In_2O_3	1910
La_2O_3	2315
MgO	2800
MnO	1815
NbO_2	1915
Nd_2O_3	2275
NiO	1960
Sc_2O_3	2450
Sm_2O_3	2310
SrO	2450
Ta_2O_5	1875
ThO_2	3250
TiO_2	1850
Ti_2O_3	2130
UO_2	2750
U_2O_3	1975
Y_2O_3	2400
Yb_2O_3	2375
ZnO	1975
ZrO_2	2700

Table 3 Melting temperatures of selected aluminates

Oxide	T_m (°C)
$BaO{\cdot}Al_2O_3$	2,000
$BeO{\cdot}Al_2O_3$	1,910
$CaO{\cdot}6Al_2O_3$	1,850
$CeO{\cdot}Al_2O_3$	2,070
$CoO{\cdot}Al_2O_3$	1,955
$FeO{\cdot}Al_2O_3$	1,820
$K_2O{\cdot}Al_2O_3$	2,260
$La_2O_3{\cdot}Al_2O_3$	2,100
$Li_2O{\cdot}5Al_2O_3$	1,975
$MgO{\cdot}Al_2O_3$	2,135
$Na_2O{\cdot}11Al_2O_3$	2,000
$NiO{\cdot}Al_2O_3$	2,020
$SrO{\cdot}Al_2O_3$	1,960
$Y_2O_3{\cdot}Al_2O_3$	1,940
$ZnO{\cdot}Al_2O_3$	1,950

Table 4 Melting temperatures of barium-containing binary refractory oxides

Oxide	T_m (°C)
$BaO{\cdot}Al_2O_3$	2,000
$3BaO{\cdot}2Dy_2O_3$	2,050
$2BaO{\cdot}GeO_2$	1,835
$6BaO{\cdot}Nb_2O_5$	1,925
$BaO{\cdot}Sc_2O_3$	2,100
$2BaO{\cdot}SiO_2$	1,820
$BaO{\cdot}ThO_2$	2,300
$2BaO{\cdot}TiO_2$	1,860
$BaO{\cdot}UO_2$	2,450
$3BaO{\cdot}2Y_2O_3$	2,160
$BaO{\cdot}ZrO_2$	2,700

Table 5 Melting temperatures of ternary refractory oxides

Oxide	T_m (°C)
$2CaO{\cdot}Y_2O_3{\cdot}Al_2O_3$	1,810
$Na_2O{\cdot}9Y_2O_3{\cdot}12SiO_2$	1,850
$2CaO{\cdot}Gd_2O_3{\cdot}Al_2O_3$	1,830
$3Ga_2O_3{\cdot}2Sc_2O_3{\cdot}3Al_2O_3$	1,850
$ZnO{\cdot}ZrO_2{\cdot}SiO_2$	2,080

normally be expected to be refractory such as those containing potassium oxide, sodium oxide, and even lithium oxide. Individually, oxides such as Li_2O, Na_2O, and K_2O would never be considered refractory, but combined with aluminum oxide they form refractory compounds.

The binary oxides listed in Table 4 were intended as a compilation that is similar to what was presented in Table 3. However, in this case barium oxide was chosen as one component of the binary system. Barium oxide is refractory (Table 2) and forms

binary refractory compounds in a number of different families, include aluminates, silicates, titanates, and zirconates. Although not absolute, it is common for an oxide that is refractory in one family of oxides to be refractory in others as well.

Looking toward the future, it is likely that the current trends in production and use of high temperature materials will continue. The users of high temperature structural materials continually push for higher use temperatures and improved component lifetime. As use temperatures increase, it is likely that alternate materials that are now considered exotic will have to be developed; this development will be application specific and will occur at a rate that often lags the rate of process development. Consider the thoughts of a steel mill operator from the early 1900s if he had been told that in 50 years his plant would use basic refractories costing orders of magnitude more than fireclay brick. Other developments that are likely in the refractory materials field are the increased use of multiphase materials and coatings. Both technologies offer the promise of unique combinations of physical and mechanical properties that are not available in single-phase materials. For example, a multiphase engineered material could be constructed to have the wear resistance of a hard ceramic with the thermal conductivity and thermal shock resistance of a metal. The possible combinations of properties are nearly endless, but development of these materials requires knowledge of interactions at bimaterial interfaces, tailoring of thermal expansion coefficients, and development of cost-effective processing routes.

The purpose of this chapter is to describe the properties and applications for refractory oxides. The sections that follow describe applications, review fundamental chemical and physical aspects, introduce processing methods, list important physical properties, and discuss materials selection criteria for refractory oxides. The organization of this chapter reflects that the performance of ceramic materials depend on interrelationships among structure, processing, and inherent properties.

2 Applications

Oxides are used by refractory and structural ceramics manufacturers to produce materials that are used in a wide variety of industries. Even with the reduced production of steel in the US, the industry continues to be the largest (in terms of tonnage) consumer of refractory products. The high temperatures required for domestic steel production coupled with increasingly stringent performance demands and ever-present cost concerns continue to drive development of new products. Annually, the steel industry consumes about one-half of the World's refractory materials. The next two largest consumers of refractories, the aluminum and the glass industries, only account for about 20% of the refractory materials produced.

Remaining production and usage is distributed over a host of industries, many of which are not commonly known. Others include nonferrous metal producers (copper, lead, zinc, etc.), the cement industry, petroleum and hydrocarbon refineries, chemical producers, pulp and paper, food production-related industries; anything involving heat and/or hot products. Although only a minor consumer, NASA utilizes refractory tiles to protect astronauts from the harsh conditions that exist on operation of the space shuttle and a refractory brick pad to manage the heat load associated with launch.

The specific application defines the type of refractory material that can be utilized not only by property requirements but also by cost requirements. Each of the industries mentioned balances refractory performance with refractory cost. At times higher quality oxide refractories are abandoned in favor of less costly, but also less affective alternatives. As these industries continue to evolve to higher and higher production temperatures, acceptable lower cost alternatives will become increasingly less available.

3 Fundamental Explanations

The properties of metal oxide compounds depend on the individual atoms present, the nature of the bonding between the atoms, and the crystalline structure of the resulting compound. Materials engineers are concerned with the physical manifestations of bonding and crystal structure, meaning macroscopic properties such as elastic modulus and coefficient of thermal expansion, rather than the nature of the interactions among atoms. However, the ability to tailor material behavior and to design compositions and microstructures for specific applications requires an understanding of the fundamental physical and chemical principles that control bonding and crystal structure. To address these points, this section provides a brief review of atomic structure and bonding, crystal structure, and the resulting macroscopic behavior as they pertain to oxide ceramics.

3.1 Atomic Structure and Bonding

On the atomic level, the arrangement of electrons surrounding a nucleus determines how a particular atom will interact with other atoms [12]. The modern understanding of electronic structure is built on the concept of the Bohr atom extended to atoms with many electrons using the principles of quantum mechanics [13]. Each electron that surrounds a particular atom has a set of four quantum numbers that designates its shell (principal quantum number $n = 1, 2, 3$, etc.), its orbital (l = integer with values ranging from 0 to $n - 1$ representing the s, p, d, and f orbitals), its orientation (m_l = integer with values from −l to +l), and its spin ($m_s = +1/2$ or $-1/2$). By the Pauli exclusion principal, each electron surrounding an atom has a unique set of four quantum numbers [14]. Standard versions of the periodic table are arranged in rows according to the electronic shell that is filled as the atomic number increases [15]. For example, atoms in the first row of the periodic table (H and He) have electrons in the first shell ($n = 1$). The increasing number of species in the lower rows of the periodic table results from the increased number of orbitals available for occupancy as n, the principal quantum number, increases. The columns represent groups of atoms with the same outer shell configuration. For example, the atoms in column IA (H, Li, Na, K, etc.) have one electron in the s orbital of the outermost shell.

The outermost electron shell surrounding an atom is referred to as its valence shell and it is the valence shell electrons that participate in chemical bonding [12]. Most often, it is the s and p orbital electrons (orbital quantum numbers 0 and 1) that affect the strength and directionality of chemical bonds [13]. When bonding, atoms minimize

their energy by gaining, losing, or sharing electrons in an attempt to attain the electronic structure of the inert gas with the closest atomic number. When atoms gain or lose electrons they become ions. Ions with opposite charges form what are termed ionic bonds. If electrons are shared, directional covalent bonds are formed. Conversely, ionic bonding is nondirectional and the resulting solids tend to have high (6, 8, or 12) cation coordination numbers. For example, CsCl is an ionic compound composed of Cs^+ and Cl^- ions. Each Cs^+ cation is surrounded by eight Cl^- anions. Covalent bonds are directional based on the shape of the electron orbitals or the type of hybrid orbital that is formed to facilitate electron sharing [13]. Covalent compounds tend to have lower cation coordination numbers (3 or 4) compared with ionic compounds. An example of a covalent compound is SiC, in which each Si atom is bound to four C atoms and the angle between each bond is ~109°, and the angle of separation for sp^3 hybrid orbitals that is also known as the tetrahedral angle. In real oxide compounds, the bonds have both ionic and covalent characteristics. These bonds are referred to as iono-covalent or polar covalent [13, 16]. The degree of ionic character can be estimated using a variety of means including Pauling's electronegativity scale, Sanderson's model, or Mooser-Pearson plots [13]. Oxides are not generally close-packed like compounds that are predominantly ionic, but are not as open as highly covalent compounds.

Regardless of the type of chemical bond that forms, the net force between two chemically bound atoms results from electrostatic attraction [16]. The attractive component, E_{attr}, of the total bond energy between two atoms is a function of the distance between them, r. The normal form of the attractive force, based on Coulomb's law, for ionic crystals is

$$E_{attr} = \frac{z_1 z_2 e^2}{4\pi\varepsilon_0 r}, \tag{1}$$

where z_1 and z_2 are the valences of the two atoms, e is the charge on an electron (1.602×10^{-19} C), and ε_0 is the permittivity of free space (8.854×10^{-12} C^2 N^{-1} m^{-2}).

The attractive energy acts over long ranges and can take slightly different forms for covalent bonding [13]. Without a repulsive force to balance the attractive force, all of the atoms in the universe would eventually be drawn into a single mass of infinite density. Fortunately, as atoms approach each other, a short-range electrostatic repulsion builds due to the overlap of the charge distributions from the two atoms [15]. Most often, the repulsive energy is expressed as the Born repulsion:

$$E_{rep} = \frac{B}{r^n}, \tag{2}$$

where B is an empirical constant and n is the Born exponent, also an empirical constant, usually between 6 and 12.

The net energy between two atoms is the sum of the attractive and repulsive energies [15]. The equilibrium atomic separation, r_0, occurs at the point where the net energy shows a maximum in attraction. The value of r_0 can be calculated by taking the first derivative of the net energy, setting it equal to zero, and solving for r. A representative plot of the attractive, repulsive, and net energies is shown in Fig. 2. The magnitude of the maximum in the attractive energy determines the bond strength and, therefore, the lattice energy, of a crystal. Considering compounds with the same structure, differences in lattice energy affect macroscopic properties [13]. An example comparing the lattice energies, melting temperatures, and thermal expansion coefficients of alkaline

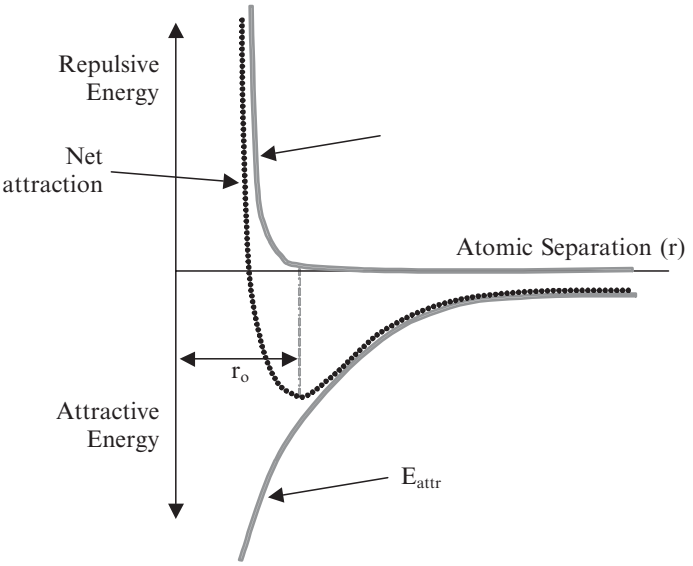

Fig. 2 Attractive, repulsive, and net interatomic energy as a function of interatomic separation

Table 6 Lattice energy, melting temperature, thermal expansion, and modulus for alkaline earth oxides with the rock salt structure

	Lattice energy (kJ mol^{-1})	Melting temperature (°C)	Coefficient of thermal expansion (ppm$°C^{-1}$)
MgO	3,938	2,852	10.5
CaO	3,566	2,614	11.2
SrO	3,369	2,430	14.2

earth oxides that have the rock salt structure (MgO, CaO, and SrO) is outlined in Table 6 [13, 17, 18]. As observed by the trend in the data, melting temperature tends to increase and thermal expansion coefficient tends to decrease as the cohesive force, expressed as the lattice energy in this example, increases.

3.2 Crystal Structure

On the nanometer level, crystal structures are symmetric arrangements of molecules (bound atoms) in three-dimensional space [19]. Driven purely by energy minimization, countless manifestations of symmetry are found in nature ranging from the arrangement of atoms in unit cells and water molecules in snowflakes to the facets of crystals such as quartz and diamond [20]. For a crystal constructed of identical molecules, the positions of all of the molecules in the structure can be predicted using four basic symmetry elements: (1) centers of symmetry; (2) two, three, four, or sixfold rotational axes; (3) mirror or reflection planes; or (4) combinations of a symmetry centers and rotational axes [21]. Combined with the constraint that space must be filled by the

resulting structural units, the symmetry elements can be used to construct structures that make up the seven basic crystal systems (cubic, hexagonal, rhombahedral, tetragonal, orthorhombic, monoclinic, and triclinic). Within the crystal systems, increasingly finer divisions of symmetry can be defined using Bravais lattices, crystal classes, or space groups (Table 7) [22]. A detailed description of how the symmetry elements relate to this hierarchy can be found in many texts on crystallography [19, 23], X-ray diffraction [21, 22], or mineralogy [20, 24]. As an aside, the convention is to name crystal structures after the mineral for which the positions of the atoms were first confirmed [16]. Thus, compounds showing face-centered cubic symmetry and belonging to the Fm3m space group are referred to as the rock salt structure, since NaCl was the first mineral proven to have this structure.

For oxide compounds, the particular crystal structure that is formed is related to the composition, the relative sizes of the atoms, and the tendency toward ionic or covalent bonding [16]. The composition of a pure crystalline material or more precisely the stoichiometry of the compound limits the possible crystal structures [13]. For example, a compound with a cation to oxygen ratio of 2:3 like Al_2O_3 cannot crystallize into the same type of structure as a compound with a cation to oxygen ratio of 1:1 like MgO [16]. The cation to oxygen ratio is constrained by the requirement that electrical neutrality be maintained. The ratio of the sizes of the cation (r_c) to the radius of the oxygen anion (r_a) also affects the types of structures that can form. As the size of the cation increases relative to oxygen, more oxygen ions can be packed around the cation center [16]. The possible coordination numbers and critical r_c/r_a ratios are given in Table 8 along with the resulting structure types [1]. Finally, the bond character also affects the crystal structure. For highly covalent crystals, the hybridization of the

Table 7 Hierarchical organization of crystal structures

Crystal system	Possible Bravais lattices	Crystal classes or point groups	Number of space groups
Cubic	P, I, F[a]	5	36
Hexagonal	P	7	27
Trigonal	P	5	25
Tetragonal	P, I	7	68
Orthorhombic	P, C, I, F	3	59
Monoclinic	P, C	3	13
Triclinic	P	2	2
7	14	32	230

[a]*P* primitive; *C* end centered; *I* body centered; *F* face centered

Table 8 Critical cation to anion radius ratios for stability various coordination environments

r_c/r_a	Coordination number	Configuration	Example
$0 \geq r_c/r_a > 0.155$	2	Linear	CO_2
$0.155 \geq r_c/r_a > 0.225$	3	Triangle	O in rutile
$0.225 \geq r_c/r_a > 0.414$	4	Tetrahedron	Wurtzite
$0.414 \geq r_c/r_a > 0.732$	6	Octahedron	Rock salt
$0.732 \geq r_c/r_a > 1.0$	8	Cubic	Fluorite
$1.0 \geq r_c/r_a$	12	Cuboctahedron	A site in Perovskite

valence shell orbitals is often the determining factor in crystal structure [16]. For example, SiC has a radius ratio of 1:6, but it crystallizes into the wurtzite structure (tetrahedral coordination) because of the strong covalent nature of the bonds [13]. A number of methods exist to predict structures including radius ratios [16], Pauling's rules [25], and Mooser-Pearson plots [13].

A majority of the important oxide ceramics fall into a few particular structure types. One omission from this review is the structure of silicates, which can be found in many ceramics [1, 26] or mineralogy [19, 20] texts. Silicate structures are composed of silicon–oxygen tetrahedral that form a variety of chain and network type structures depending on whether the tetrahedra share corners, edges, or faces. For most nonsilicate ceramics, the crystal structures are variations of either the face-centered cubic (FCC) lattice or a hexagonal close-packed (HCP) lattice with different cation and anion occupancies of the available sites [25]. Common structure names, examples of compounds with those structures, site occupancies, and coordination numbers are summarized in Tables 9 and 10 for FCC and HCP-based structures [13, 25]. The FCC-based structures are rock salt, fluorite, anti-fluorite, perovskite, and spinel. The HCP-based structures are wurtzite, rutile, and corundum.

3.3 Macroscopic Behavior

The macroscopic behavior of refractory oxides is controlled by both the bonding and crystal structure. In particular, the mechanical response and electrical behavior of materials are interpreted in terms of the symmetry of the constituent crystals using matrix or tensor algebra [27]. Other characteristics such as melting temperature and

Table 9 FCC-based crystal structures

Structure	Stoichiometry	Cation coordination	Oxygen coordination	Examples	Common characteristics
Rock salt	MO	6	6	MgO, CaO, NiO, FeO	
Fluorite	MO_2	8	4	ZrO_2, ThO_2, CeO_2	Oxygen ion conduction
Anti-fluorite	M_2O	4	8	Na_2O, Li_2O, K_2O	Fluxes, prone to hydration
Perovskite	ABO_3	$A = 12$, $B = 6$	6	$PbTiO_3$, $BaTiO_3$	High dielectric constant
Spinel	AB_2O_4	$A = 4$, $B = 6$	4	$MgAl_2O_4$, $MnFe_2O_4$	High solid solubility

Table 10 HCP-based crystal structures

Structure	Stoichiometry	Cation coordination	Oxygen coordination	Examples	Common characteristics
Wurtzite	MO	4	4	ZnO, BeO	
Rutile	MO_2	6	3	TiO_2, MnO_2,	Multiple cation oxidation states
Corundum	M_2O_3	6	4	Al_2O_3, Cr_2O_3	Highly refractory

Table 11 Melting temperature [9], thermal expansion coefficient (0–1,000°C) [1], thermal conductivity (25°C) [17], elastic modulus [60], and heat capacity for some common refractory oxides

Oxide	T_m (°C)	CTE (ppm per °C)	k (W m^{-1} K^{-1})	E (GPa)	C_P (J mol^{-1} K^{-1})
Fused SiO_2	1,460	0.5	2	72	42.2
Quartz	1,460	10.7	13	83	56.2
TiO_2	1,850	7.3	8.4	290	36.9
$3Al_2O_3{\cdot}2SiO_2$	1,850	5.3	6.5	220	77.1
Al_2O_3	2,020	8.8	36.2	390	78.7
$MgAl_2O_4$	2,135	7.6	17	239	324
ZrO_2	2,700	10	2.3	253	55.1
MgO	2,800	13.5	48.5	300	115.8

stability at elevated temperature are not directional and, therefore, cannot be manipulated in the same manner. However, nondirectional properties are still affected by structure in that some crystal structures are inherently more resistant to change than others. For example, structures in which some crystallographic sites are unoccupied, such as spinel, have a much higher solubility for other cations than more close-packed structures like corundum.

Phase diagrams are perhaps the most powerful tool of the materials engineer who needs to choose oxide ceramics for use at high temperature. Phase diagrams are graphical representations of the phases that are stable as a function of temperature, pressure, and composition [28, 29]. Phase diagrams can be used to determine whether a particular compound melts at a specific temperature (congruent melting), decomposes to other compounds while partially melting (incongruent melting), or reacts with another component in the system. A wide variety of phase diagrams for oxide systems are available in various compilations [9–11]. When phase diagrams are not available, behavior can be predicted with at least moderate success, using commercial programs such as FACT-SAGE [30] or using the CALPHAD methodology [31].

Considering potential applications for refractory oxides, phase diagrams also provide useful information on interactions among materials at high temperatures that might limit performance in certain gaseous atmospheres or in contact with specific liquid or solid materials. Interactions can range from the formation of low melting eutectics to reactions that form new compounds. As an example of the former, consider the effect of impurities in SiO_2. Pure SiO_2 has an equilibrium melting temperature of 1713°C [1]. All SiO_2, whether it is naturally occurring or prepared by other means, contains some impurities. If the presence of trace quantities of Na_2O are considered, a liquid phase would form at ~800°C, the SiO_2–$Na_2O{\cdot}2SiO_2$ eutectic [32]. For small impurity levels, the amount of liquid increases as the amount of the second phase increases. If sufficient liquid forms to cause deformation of the component, the use temperature of silica will be reduced drastically. Eutectic liquids form when the Gibbs' energy released by mixing of the liquid components (entropic) overcomes the energy barrier (enthalpic) to melting of the unmixed solids.

Phase diagrams can also be used as an aid for material selection of oxide compounds that can be used at high temperature. Examination of diagrams (summarized in Tables 2–5) reveals that oxide compounds with melting temperatures above 1800°C are predominantly single metal oxides (e.g., Al_2O_3 or TiO_2) or binary oxides

(e.g., $MgO{\cdot}Al_2O_3$ or $BaO{\cdot}ZrO_2$). Very few ternary oxides have high melting temperatures. The complex site occupancies and arrangements necessary to accommodate three or more cations in a single crystal structure reduce the melting temperature of ternary compounds. Upon examining ternary phase diagrams, it becomes apparent that ternary eutectic temperatures are always lower than the three binary eutectic temperatures in the corresponding binary systems. As with the binary eutectic, addition of a third component drives the eutectic temperature lower since mixing of the liquid phase components becomes more energetically favorable as the number of components increases.

It is important to distinguish between melting temperature and melting range, as the former is a fundamental property of an oxide, while the latter is a macroscopic behavior that dictates use conditions and tolerable impurity limits. Melting temperature is fairly easily understood requiring little more than observing melting of an ice cube (solid H_2O). However, only very pure substances exhibit a true melting temperature. Practical materials, except for the most pure versions (devoid of significant levels of impurity), exhibit a melting range that is defined by the macroscopic environment in which the materials exist.

In a binary combination of two oxides (e.g., alumina and silica), small additions of the second oxide result in the onset of melting at a eutectic temperature that is below the melting temperature for the pure components. For the alumina–silica system, two eutectic compositions exist depending on the overall chemistry of the mixture. For the silica-rich eutectic, all compositions between ~1 wt% and ~70 wt% alumina have an identical temperature for the onset of melting; only the amount of liquid formed will vary with composition. This temperature defines the low end of the melting range, while the temperature at which all of the material is molten (i.e., the liquidus temperature) defines the high end.

Melting range can have a profound impact on performance as liquid formation can lead to shrinkage of the refractory, reaction with the contained product, high temperature softening and flow (especially under pressure), etc. The viscosity behavior of the liquid itself is also important as highly viscous fluids behave very similarly to solids so considerably more can be present before problems occur.

4 Processing

The intrinsic properties of materials depend on bonding and crystal structure. For ceramics, the microstructure that results from the processing cycle also has a strong influence on performance. Because a majority of commercial ceramic parts are fabricated from fine powdered precursors, microstructure development during densification must be understood to control the performance of the final part. The steps in the process include powder synthesis, consolidation of powders/shaping, and densification. Powder synthesis methods range from the traditional “heat and beat” approach that uses repeated calcination and mechanical grinding steps [33] to more sophisticated reaction-based and chemical preparation methods [34]. Powder synthesis has been the subject of technical articles and reviews and will not be discussed further in this chapter. Likewise, the consolidation methods used to shape powders such as dry pressing and isostatic pressing are well documented elsewhere [35]. This section will review some key issues related to microstructure development during densification. Typical

microstructures produced by solid-state sintering will be contrasted with those formed by liquid phase sintering to highlight the potential effects on performance.

4.1 Solid-State Sintering

Solid-state sintering is the preferred method used to produce fine-grained ceramics with high relative density because of process simplicity. A large variety of high purity precursor powders are commercially available with common refractory oxides such as Al_2O_3, ZrO_2, MgO, and others produced in industrially significant quantities. The process of sintering will only be briefly reviewed here since several excellent texts [36, 37] and overviews are available [38, 39]. In addition, numerous papers have been published on the sintering of specific ceramic compounds.

During solid-state sintering, porosity in powder compacts is reduced from 40 to 60 vol% in green bodies to values that can approach zero in finished parts [35]. As the porosity is removed, the volume of the part decreases while modulus and mechanical strength increase [1]. Solid-state sintering is driven by the reduction of surface free energy that occurs when high energy solid-vapor interfaces (e.g., particle surfaces) are replaced by lower energy solid-solid interfaces (e.g., grain boundaries) [37]. For academic study, the sintering process is divided into stages: (1) initial sintering, (2) intermediate sintering, and (3) final sintering [37]. These stages can be defined in terms of physical changes in the compacts such as grain size or total volume, variations in physical properties such as relative density, or differences in mechanical properties such as moduli [37]. The sintering rate, ultimate relative density, and final grain size are affected by the particular oxide chemistry that makes up the compact, its initial particle size, and the efficiency of particle packing after consolidation. In general, effective solid-state sintering is limited to powders with relatively fine (~10 μm or less) particle size.

Densification of powder compacts requires mass transport. In solid-state sintering, material is transported from the bulk or the surface of particles into pores. To overcome kinetic limitations and promote mobility of atoms, a powder compact is heated to a significant fraction of its melting temperature. Sintering temperatures for single phase oxides typically fall in the range of 0.75–0.90 of the melting temperature (T_m). For example, mullite (incongruent melting point 1890°C or 2,163 K [40]) with an initial particle size of approximately 0.2 μm can be sintered to ~98% relative density by heating to 1600°C (1,723 K or 0.80 T_m) for 2 h [41, 42]. The resulting ceramic had a final grain size of approximately 1 μm (Fig. 3) and a microstructure typical of solid state sintered, fine grained ceramics.

Sintering temperature and rate are also affected by particle size. Precursor powders with a “fine” grain size reach the same density at lower temperatures compared with “coarse” grained powders [35]. Smaller particles have a greater surface area to volume ratio and, therefore, a higher driving force for densification, which can lower the temperature required for densification [1]. In addition to precursor powder particle size, the packing of particles prior to sintering affects densification. Nonuniform particle packing can result in the formation of stable pores in fired microstructures [35]. As the pore size approaches the grain size, the driving force for pore removal approaches zero; pores that are larger than the grains are, therefore, stabilized due to a lack of driving force for removal [37]. Stable pore formation is especially problematic when

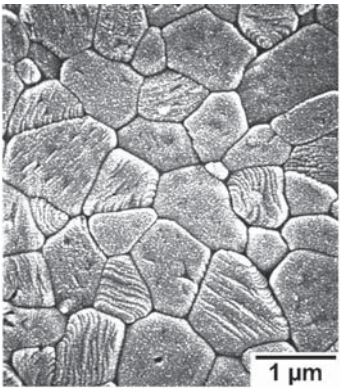

Fig. 3 Microstructure of a solid-state sintered mullite ceramic with a relative density >99%. The ceramic had equiaxed grains with a grain size of ~1 µm and no apparent glassy phase

nano-sized particles are employed because of their propensity toward formation of hard agglomerates.

The grain size of a sintered ceramic affects its performance. During solid-state sintering, grains grow during the final stage of sintering as full density is approached [43]. As with the densification process, grain growth is also driven by a reduction in surface energy; however, elimination of grain boundaries (solid-solid interfaces) in dense solids is less energetically favorable than the elimination of free surfaces (solid-vapor interfaces) in porous compacts [1]. The grain size required to achieve the performance requirements for a particular application may be smaller or larger than the grain size that would result from the optimal heat treatment. Grain growth can be altered by changing the time and temperature of the heat treatment [37]. In many cases, trace additives or dopants can be used to further modify grain growth [38]. Some dopants dissolve into the matrix altering its defect chemistry and thereby affecting material transport rates. Other dopants remain as discrete particles that affect grain growth simply by their presence in grain boundaries. The classic example of a particulate dopant that inhibits grain growth while promoting sintering is the addition of MgO to Al_2O_3. When α-Al_2O_3 is sintered at 1600°C in air, the average grain size is ~5.0 µm and a density of ~97% is achieved [44]. For the same α-Al_2O_3 doped with 250 ppm MgO sintered under the same conditions to the same density, the grain size is only ~3.5 µm [16].

4.2 Liquid Phase Sintering

Liquid phase sintering is a densification process in which a liquid phase increases the consolidation rate by facilitating particle rearrangement, enhancing transport kinetics, or both [16]. The modern practice of liquid phase sintering evolved from the vitrification of traditional ceramic ware [45, 46]. During vitrification of clay-based ceramics, heating induces the formation of a high viscosity siliceous liquid phase [1]. The liquid facilitates the dissolution of the remaining solid and the subsequent precipitation of primary mullite crystals with a needle-like morphology [47]. The fraction of liquid depends upon the particular batch composition and the firing temperature, but can be well over 50 vol% for common triaxial whitewares [45]. During vitrification, the

porous powder compact undergoes physical changes (shrinkage, pore removal) and chemical reactions (conversion of meta-kaolin to mullite, glass formation). The final vitrified body is generally free of pores and contains primary mullite that is formed during vitrification, secondary mullite that is formed by precipitation from the liquid during cooling, solidified glass, plus any inert fillers such as quartz that may have been added to the batch [47]. The glassy phase serves as a bonding phase cementing the mullite crystals and fillers into a dense, strong ceramic [1]. Unlike solid-state sintering, liquid phase sintering is an effective means for densification of large grain (10 μm or greater) materials.

The modern practice of liquid phase sintering uses additives to facilitate liquid phase formation [48]. Effective liquid phase sintering minimizes liquid formation to avoid unintended deformation during densification [49]. Liquid contents as low as 3–5 vol% are possible for well-designed liquid phase sintering operations [37]. To promote densification, the liquid must form in appreciable quantities at the desired sintering temperature, it must wet the matrix, and it must be able to dissolve the matrix [49]. As with vitrification, densification during liquid phase sintering occurs by particle rearrangement and solution precipitation, which are then followed by nondensifying grain coarsening through Ostwald ripening [37]. Upon cooling, the liquid may form a glass or a crystalline phase. The solidified liquid can form a continuous film that surrounds the grains, an interpenetrating phase in the form of ligaments along grain boundaries, or an isolated phase that retreats to triple-grain junctions [1]. Liquid penetration along the grain boundaries is a function of the ratio of solid–solid interfacial energy to solid–liquid interfacial energy, which is commonly expressed as the dihedral angle [37]. To enhance performance at elevated temperatures, the amount of the residual second phase should be minimized if it is glassy upon cooling. Alternatively, some liquid phase sintering aids are designed to convert to crystalline phases that resist deformation. In either case, the resulting ceramic cannot generally operate above the temperature at which any glassy phase softens or the lower end of the melting range. In many instances, use temperatures are substantially below these limits. A representative liquid phase sintered microstructure, in this case for a mullite ceramic, has both a major phase and a solidified liquid (Fig. 4). The grain size in the liquid phase sintered ceramic is nearly an order of magnitude greater than in the solid-state sintered ceramic because of increased particle coarsening.

Liquid phase sintering processes can be designed for ceramic systems (and metallic ones for that matter) with the aid of phase diagrams [37]. The first step in designing

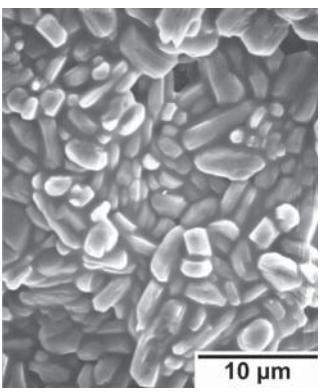

Fig. 4 Microstructure of a liquid phase sintered mullite ceramic with a relative density >99%. The ceramic had elongated grains with a grain size of >5 μm and had a residual glassy phase surrounding the mullite grains

the liquid phase sintering process is to determine a range of compositions for the proposed additives that will promote liquid formation at the desired sintering temperature. This can be done using the appropriate binary, ternary, or higher order phase diagrams. Next, the composition of the liquid phase, after it becomes saturated with the matrix phase, can be predicted by constructing a join between the additive composition and matrix composition. Finally, the amount and composition of the phases that will be present after processing can be predicted by analyzing the cooling path for the matrix saturated liquid phase. One common example is the densification of α-Al_2O_3 with the aid of a $CaO–SiO_2$ glass [50]. Using the $CaO–SiO_2–Al_2O_3$ ternary phase diagram [51], the first choice may be to select the $CaO–SiO_2$ composition that results in the minimum melting temperature (64 wt% SiO_2, 36 wt% CaO, which is the binary eutectic composition that melts at 1,426°C). However, analysis of the resulting liquid phase (19 wt% CaO, 34 wt% SiO_2, 47 wt% Al_2O_3) indicates that $CaO{\cdot}6Al_2O_3$, $2CaO{\cdot}Al_2O_3{\cdot}SiO_2$, and $CaO{\cdot}Al_2O_3{\cdot}2SiO_2$ will form upon final solidification by peritectic reaction at 1,380°C. For example, the Al_2O_3-saturated liquid composition lies in the $CaO{\cdot}6Al_2O_3$–$2CaO{\cdot}Al_2O_3{\cdot}SiO_2$–$CaO{\cdot}Al_2O_3{\cdot}2SiO_2$ compositional triangle. The resulting ceramic would contain 91.5 wt% α-Al_2O_3 for a composition containing a 4.0 wt% sintering aid addition. To increase the α-Al_2O_3 content of the final product, the initial additive composition can be shifted to 67 wt% SiO_2 so that a liquid phase containing 19 wt% CaO, 36 wt% SiO_2, 45 wt% Al_2O_3 forms when equilibrium is reached at 1,600°C. Upon cooling, Al_2O_3, $CaO{\cdot}6Al_2O_3$, and $CaO{\cdot}Al_2O_3{\cdot}2SiO_2$ will form by peritectic reaction at 1,495°C, increasing the resulting α-Al_2O_3 content of the final ceramic to 93.7 wt% for a composition containing a 4.0 wt% sintering aid addition. This change in composition also increases the temperature of first liquid formation by 115°C thereby allowing the ceramic to be used in higher temperature applications.

5 Properties

The critical material properties for refractory oxides are dictated by a given application. In some applications, thermal expansion and strength may be most important while in other situations melting temperature and thermal conductivity are important. In general, the most important material properties for refractory oxides include melting temperature, thermal expansion coefficient, thermal diffusivity and conductivity, elastic modulus, and heat capacity.

5.1 Melting Temperature

Melting temperature (T_m in units of °C or K) and melting range were discussed previously. The former will be the higher of the two and represents the temperature at which the phase pure oxide melts. As has been discussed, melting temperature data for selected oxides are included in Tables 2–5. A review of the literature also yields melting temperatures for many thousands of oxides that would not be classified as refractory.

During application of refractory oxides, melting range is typically more important than melting temperature. Softening point is defined as the temperature at which a

material begins to deform under its own load. With phase pure oxide systems, melting temperature and softening point are equivalent; however, in most practical systems impurities are inherent. These impurities lead to low melting point eutectic formation that can lower the maximum use temperature of the oxide.

Phase equilibria diagrams yield an estimate of the softening point for a refractory oxide. Considering the binary phase diagram for the oxide and the predominant impurity, the invariant temperature (eutectic, peritectic, or monotectic) or the invariant that is closest to the refractory oxide composition indicates the lowest temperature that will result in liquid formation and, therefore, the lowest possible softening point. Although an appropriate ternary phase diagram is required, the situation is only slightly more complex when two impurities are present in significant concentrations. In that situation, initial liquid formation is defined by the invariant point for the Alkemade triangle between the refractory oxide and the two impurities. For example, pure SiO_2 has an equilibrium melting temperature of 1713°C. The addition of Na_2O reduces the eutectic temperature to ~800°C at the SiO_2-rich end of the diagram. Adding a third oxide, K_2O, reduces the eutectic temperature to ~540°C at the SiO_2-rich end of the diagram.

5.2 Thermal Expansion

Thermal expansion is the change in specific volume of a material as it is heated. The linear coefficient of thermal expansion (α with units of inverse temperature) can be expressed as the change in length of an object, normalized by its original length, for a given temperature change (3):

$$\alpha = \left(\frac{\Delta L}{L}\right)\left(\frac{1}{\Delta T}\right) \tag{3}$$

where ΔL is the change in length for a given temperature change (m), L is the original length (m), and ΔT is the change in temperature (K).

In general, all materials have a positive thermal expansion coefficient; that is they increase in volume when heated. Thermal expansion results from thermal excitation of the atoms that compose the material [16]. At absolute zero, atoms are at rest at their equilibrium positions (i.e., at r_0 in Fig. 1). As they are heated, thermal energy causes the atoms to vibrate around their equilibrium positions. The amplitude of vibration increases as heating is continued. Asymmetry in the shape of the potential well causes the average interatomic distance to increase as temperature increases, leading to an overall increase in volume [15].

The importance of considering thermal expansion cannot be underestimated. Ignoring thermal expansion or incorrectly accounting for thermal dilations can have serious consequences. Consider a vessel that is ~3 m (~10 ft) in diameter insulated with a zirconia refractory. Assuming a linear coefficient of thermal expansion of 13 ppm K^{-1}, heating the lining from room temperature to 1600°C the inside surface of the lining would grow by about 5 cm (~2 in.). To compensate for expansion in large systems, it is common to leave expansion joints spaced at regular intervals. When temperature is increased, the refractory material will shift into the open space preventing potential problems.

5.3 Thermal Diffusivity/Conductivity

Thermal conductivity (k with units W m^{-1} K^{-1}) describes the ability of a material to transport thermal energy because of temperature gradient. Steady-state thermal conductivity is a constant of proportionality between the heat flux (time rate of heat flow per unit area) through a solid and the imposed temperature gradient as described by (4) [52]:

$$\frac{Q}{A} = k\,\frac{\Delta T}{x}, \tag{4}$$

where Q is the heat flow (J s^{-1} or W), A is cross sectional area (m^2), k is thermal conductivity (W m^{-1} K^{-1}), ΔT is temperature gradient (K), and x is distance (m).

In electrically insulating solids, heat is transferred in the form of elastic waves or phonons [1]. Anything that affects the propagation of the phonons through the solid affects the thermal conductivity of the solid. In a pure crystalline ceramic, the intrinsic thermal conductivity is limited by the energy dissipated during phonon–phonon collisions or so-called Umklapp processes [15]. Commonly, the intrinsic thermal conductivity of solids is described by (5).

$$k = \frac{1}{3}\,Cvl, \tag{5}$$

where C isthe heat capacity per unit volume (J m^{-3} K^{-1}), v is the phonon velocity (m s^{-1}), and l is phonon mean free path (m).

Phonon velocity and mean free path are difficult to measure accurately in polycrystalline materials, so (5) is normally restricted to theoretical predictions. The values of thermal conductivity observed in polycrystalline ceramics are often significantly less than the intrinsic values predicted or those measured for single crystals. Specimen characteristics such as temperature, impurities, grain size, porosity, and preferred orientation affect the phonon mean free path thereby changing thermal conductivity [1]. Though not an oxide, this effect is pronounced in aluminum nitride. The intrinsic thermal conductivity of AlN is 280 W m^{-1} K^{-1} [16], but thermal conductivities in the range of 50–150 W m^{-1} K^{-1} are often observed in sintered materials because of the presence of grain boundaries and second phases [53].

The thermal conductivity of large grained (100 µm or more) ceramics can be determined by direct measurement techniques described in ASTM standards C 201-93 (Standard Test Method for Thermal Conductivity of Refractories), C 1113-99 (Standard Test Method for Thermal Conductivity of Refractories by Hot Wire), and E 1225-99 (Standard Test Method for Thermal Conductivity of Solids by Means of the Guarded-Comparative-Longitudinal Heat Flow Technique). These methods lend themselves to quality control-type assessment of the thermal conductivity of macroscopic parts in standard shapes (e.g., 9 in. straight brick or monolithic materials cast to specific dimensions). The sizes prescribed by these standards insure that the specimen thickness is sufficient to reflect the effects of grain boundaries, pores, and other specimen characteristics. The relative error of the techniques ranges from ~10 to ~30% depending on the material and technique. This degree of precision is normally sufficient for material selection and design calculations. Some common design considerations influenced by thermal conductivity include cold-face temperature, interface temperatures between working lining and insulating lining materials, heat loss, and estimating

the required thickness for each component in a system. For example, the heat flux through a refractory material can be calculated using (4). Assuming a characteristic thermal conductivity for an insulating firebrick of 0.25 W m^{-1} K^{-1} at the mean temperature of the wall, a heat flow of 5000 J s^{-1} would be predicted per square meter of area for a hot face temperature of 1200°C (1473 K), a cold face temperature of 200°C (473 K), and a wall thickness of 5 cm (0.05 m).

For dense specimens of fine-grained (less than 100 μm) technical ceramics, the thermal conductivity can be determined with greater precision using an indirect method by which thermal diffusivity (α with units of m^2 s^{-1}) is measured and then converted to thermal conductivity. For small specimens, precise control of heat flow and accurate determination of small temperature gradients can be difficult, leading to unacceptably large error in the direct measurement of thermal conductivity of small specimens. As a consequence, determination of thermal diffusivity by impulse heating of thin specimens followed by conversion to thermal conductivity has evolved as the preferred measurement technique [54, 55]. The technique is described in ASTM standard E1461–01 (Standard Test Method of Thermal Diffusivity by the Flash Method). Measured thermal diffusivity is used to calculate thermal conductivity using (6):

$$\alpha = \frac{k}{C_p \rho} \tag{6}$$

where α is thermal diffusivity (m^2 s^{-1}), k is thermal conductivity (W $(m^{-1}$ $K)^{-1}$), C_p is heat capacity (J kg^{-1} K^{-1}), ρ is density (kg m^{-3}).

5.4 Elastic Modulus/Strength

Elastic modulus or Young's modulus (E with units of GPa) describes the response of a linear elastic material to an applied mechanical load [16]. Elastic modulus relates the applied load to the resulting strain as expressed by Hooke's law (7).

$$\sigma = E\varepsilon \tag{7}$$

where σ is the applied stress (GPa) and ε is the strain (no units).

Under an applied load, deformation of the solid requires that the atoms be moved closer together (compressive load) or farther apart (tensile load). As such, dimensional changes are related to the strength of the bonds among the atoms [8]. When the component ions of a material have high bond strengths, the material typically displays high elastic modulus and low coefficient of thermal expansion. For example, SiC has a high bond strength giving sintered α-SiC a coefficient of thermal expansion of 4.02 ppm K^{-1} and a modulus of 410 GPa [56]. Conversely, NaCl has a low bond strength resulting in a coefficient of thermal expansion of 11.0 ppm K^{-1} and a modulus of 44 GPa [16, 57]. Modulus can be measured using either acoustic methods (ASTM E 1876 Standard Test Method of Dynamics Young's Modulus, Shear Modulus, and Poisson's Ratio by Impulse Excitation of Vibration) or by directly measuring displacement as a function of an applied load using a deflectometer.

Although modulus is a fundamental material property related to the strength of the chemical bonds among atoms, the measured strength (σ with units of MPa) is affected by specimen characteristics, the testing environment, the type of test performed, and other factors. The theoretical tensile strength can be estimated as the stress required to break the chemical bonds among the atoms of a solid [57]. However, brittle materials fail at applied stresses two or more orders of magnitude below the theoretical strength values due to stress concentration around physical features of the solids such as pores, defects, grain boundaries, and edges. The Griffith criterion is often used to relate the fundamental material properties such as modulus to observed strength using specimen characteristics such as flaw size [1], although the predictions are qualitative at best. The Griffith criterion can be used to understand the statistical nature of fracture of brittle materials if the distribution of flaw sizes within a given specimen is considered [16]. Strength can be measured in many different manners ranging from compression (ASTM C1424 Standard Test Method for Monotonic Compressive Strength of Advanced Ceramics at Ambient Temperatures) to tension (ASTM C1273 Standard Test Method for Tensile Strength of Monolithic Advanced Ceramics at Ambient Temperatures). The strength of advanced ceramics is most often measured using relatively small specimens in three- or four-point bending, which determines the so-called flexural strength (ASTM C1161 Standard Test Method for Flexural Strength of Advanced Ceramics at Ambient Temperature). Because traditional refractory materials have grain sizes that approach or exceed the size of the specimens used for testing of advanced ceramics, strengths must be determined using alternate methods (ASTM C133 Standard Test Methods for Cold Crushing Strength and Modulus of Rupture of Refractories) that accommodate course grain specimens.

5.5 *Heat Capacity*

Heat capacity (C_p with units such as J mol^{-1} K^{-1} or J kg^{-1} K^{-1}) is defined as the quantity of thermal energy required to raise the temperature of a substance one degree [58]. In practice, heat capacity and the term specific heat are used almost interchangeably. For ionic solids, atoms can be modeled as centers of mass that can vibrate independently in three dimensions [59]. The vibrational energy of the atoms increases as thermal energy is added to the system. The heat capacity of all solids approaches $3N_Ak$ with temperature (where N_A is Avagadro's number and k is the Boltzmann constant) or $3R$ (where R is the ideal gas constant) per mole of atoms, the familiar Dulong-Petit law. At low temperature, the models of Einstein and Debye can be used to estimate heat capacity [15]. In practice, heat capacity in terms of energy and mass is more useful and is compiled as a function of temperature in any number of reference books [2, 3, 60]. Experimentally, heat capacity can be determined using such heat flow techniques as differential scanning calorimetry.

Heat capacity is important because it regulates the amount of energy required to raise the temperature of a thermal load (e.g., ware to be fired plus kiln furniture). Such data can be used to compute furnace efficiency, which is the ratio of fuel usage to the thermal energy requirement of a process. In addition, knowledge of heat capacities of products, kiln furniture, and refractories is essential for good furnace design.

6 Summary

Refractory oxides are an important class of materials that enable processes to exploit extreme environments. A wide variety of unary, binary, and ternary oxides can be considered refractory, based on their melting temperatures. Refractory oxides are generally prepared from powdered precursors using standard ceramic forming techniques such as casting, pressing, or extrusion, and subsequently sintered to achieve final density. In addition to chemical compatibility, the physical properties of refractory oxides such as thermal expansion coefficient, thermal conductivity, modulus of elasticity, and heat capacity must be considered when selecting an oxide for a specific application.

References

1. W.D. Kingery, H.K. Bowen, and D.R. Uhlmann, *Introduction to Ceramics*, 2nd edn., Wiley, New York, 1976.
2. M.W. Chase, Jr., *NIST-JANAF Thermochemical Tables*, 4th edn., American Institute of Physics, Woodbury, NY, 1998.
3. R.C. Weast and M.J. Astle (eds.), *Handbook of Chemistry and Physics*, 62nd edn., CRC Press, Boca Raton, 1981.
4. H. Ries, *Clays, Their Occurrence, Properties, and Uses*, 3rd edn., Wiley, New York, 1927.
5. F.H. Norton, *Refractories*, 2nd edn., McGraw-Hill, New York, 1942.
6. Harbison-Walker Refractories, *HW Handbook of Refractory Practice*, 2nd edn., Harbison-Walker Refractories, Pittsburgh, 1980.
7. TARJ, *Refractories Handbook*, The Technical Association of Refractories, Japan, Tokyo, 1998.
8. W.D. Kingery, *Introduction to Ceramics*, Wiley, New York, 1960.
9. The American Ceramic Society, *Phase Diagrams for Ceramists*, Vols. 1–13, The American Ceramic Society, Columbus/Westerville, OH, 1964–2001.
10. R.S. Roth, The American Ceramic Society (eds.), *Phase Diagrams for Electronic Ceramics I: Dielectric Ti, Nb, and Ta Oxide Systems*, The American Ceramic Society, OH, 2003.
11. H.M. Ondik and H.F. McMurdie (eds.), *Phase Diagrams for Zirconium and Zirconia Systems*, The American Ceramic Society, OH, 1998.
12. L. Pauling, *The Nature of the Chemical Bond*, 3rd edn., Cornell University Press, Ithaca, NY, 1960.
13. A.R. West, *Basic Solid State Chemistry*, 2nd edn., Wiley, Chichester, 1999.
14. H.L. Brown and H.E. LeMay, Jr., *Chemistry: The Central Science*, 2nd edn., Prentice-Hall, NJ, 1981.
15. C. Kittel, *Introduction to Solid State Physics*, 6th edn., Wiley, New York, 1986.
16. M. Barsoum, *Fundamentals of Ceramics*, McGraw Hill, New York, 1997.
17. Y.S. Touloukian, R.K. Kirby, R.E. Taylor, and T.Y.R. Lee, *Thermophysical Properties of Matter Volume 13: Thermal Expansion, Non Metallic Solids*, IFI Plenum, New York, 1977.
18. R.C. Evans, *An Introduction to Crystal Chemistry*, 2nd edn., University Press, Cambridge, 1964.
19. C. Klein and C.S. Hurlbut, Jr., *Manual of Mineralogy*, 21st edn., Wiley, New York, 1993.
20. B.D. Cullity and S.R. Stock, *Elements of X-Ray Diffraction*, 3rd edn., Prentice-Hall, NJ, 2001, pp. 31–88.
21. R. Jenkins and R.L. Snyder, *Introduction to X-Ray Powder Diffractometry*, Wiley, New York, 1996, pp. 23–46.
22. F.D. Bloss, *Crystallography and Crystal Chemistry; An Introduction*, Holt, Rinehart, and Winston, New York, 1971.
23. W.D. Nesse, *Introduction to Optical Mineralogy*, Oxford University Press, New York, 1986.

24. Y.-M. Chiang, D. Birnie, III, and W.D. Kingery, *Physical Ceramics: Principles for Ceramic Science and Engineering*, Wiley, New York, 1997, pp. 13–19.
25. F.H. Norton, *Fine Ceramics*, McGraw-Hill, New York, 1970, p. 40.
26. J.F. Nye, *Physical Properties of Crystals: Their Representation by Tensors and Matrices*, Clarendon Press, Oxford, 1985.
27. C.G. Bergeron and S.H. Risbud, *Introduction to Phase Equilibria in Ceramics*, The American Ceramic Society, Columbus, OH, 1984.
28. F.A. Hummel, *Introduction to Phase Equilibria in Ceramic Systems*, Marcel Dekker, New York, 1984.
29. Available from the Centre for Research in Computational Thermochemistry at Ecolé Polytechnique, Box 6079, Station Downtown, Montreal, Quebec, Canada.
30. CALPHAD: Computer Coupling of Phase Diagrams and Thermochemistry, The International Research Journal for Calculation of Phase Diagrams, published quarterly by Elsevier.
31. E.M. Levin, C.R. Robbins, and H.F. McMurdie, *Phase Diagrams for Ceramists,* Vol. 1, The American Ceramic Society, Columbus, OH, 1964, Figure 192.
32. G.Y. Onoda and L.L. Hench (eds.), *Ceramic Processing Before Firing*, Wiley, New York, 1978.
33. C.J. Brinker, D.E. Clark, and D.R. Ulrich (eds.), *Better Ceramics Through Chemistry*, Materials Research Society Proceedings Volume 32, North Holland, New York, 1984.
34. J.S. Reed, *Principles of Ceramics Processing*, Wiley, New York, 1995.
35. R.M. German, *Sintering Theory and Practice*, Wiley, New York, 1996.
36. M.N. Rahaman, *Ceramic Processing and Sintering*, Marcel Dekker, New York, 1995.
37. M.F. Yan, Solid state sintering, in *Ceramics and Glasses: Engineered Materials Handbook*, Vol. 4, ASM International, Materials Park, OH, 1991, pp. 270–284.
38. M.P. Harmer, Science of sintering as related to ceramic powder processing, in *Ceramic Powder Science II, Ceramic Transactions*, Vol. 1, G.L. Messing, E.R. Fuller, Jr., and H. Hausner (eds.), The American Ceramic Society, Westerville, OH, 1988, pp. 824–839.
39. F.J. Klug, S. Prochazka, and R.H. Doremus, Alumina-silica phase diagram in the mullite region, *J. Ame. Ceram. Soc.* **70**(10) 750–759 (1987).
40. W.G. Fahrenholtz, *Particle size and mixing effects on the crystallization and densification of sol-gel mullite*, Ph.D. Thesis, University of New Mexico, 1992.
41. W.G. Fahrenholtz, D.M. Smith, and J. Cesarano III, Effect of precursor particle size on the densification and crystallization behavior of mullite, *J. Am. Ceram. Soc.* **76**(2), 433–437 (1993).
42. R.J. Brook, Controlled grain growth, in *Ceramic Fabrication Processes: Treatise on Materials Science and Technology*, Vol. 9, F.F.Y. Wang (ed.), Academic Press, New York, 1976, pp. 331–364.
43. K.A. Berry and M.P. Harmer, Effect of MgO solute on microstructure development in Al_2O_3, *J. Am. Ceram Soc.* **69**(2), 143–149 (1986).
44. F.H. Norton, *Fine Ceramics*, McGraw-Hill, New York, 1970, pp. 258–280.
45. G.W. Brindley and M. Nakahira, The kaolinite-mullite reaction series: I, a survey of outstanding problems; II, metakaolin; and III, the high temperature phases, *J. Am. Ceram. Soc.* **42**(7), 311–324 (1959).
46. Y. Iqbal and W.E. Lee, Microstructural evolution in triaxial porcelain, *J. Am. Ceram. Soc.* **83**(12), 3121–3127 (2000).
47. R.M. German, *Liquid Phase Sintering*, Plenum, New York, 1985.
48. O.-H. Kwon, Liquid phase sintering, in *Ceramics and Glasses: Engineered Materials Handbook* Vol. 4, ASM International, Materials Park, OH, 1991, pp. 285–290.
49. O.-H. Kwon and G.L. Messing, Kinetic analysis of solution-precipitation during liquid-phase sintering of alumina, *J. Am. Ceram. Soc.* **73**(2), 275–281 (1990).
50. E.M. Levin, C.R. Robbins, and H.F. McMurdie (eds.), *Phase Diagrams for Ceramists,* Vol. 1, The American Ceramic Society, Columbus, OH, 1964, Figure 630.
51. R.B. Bird, W.E. Stewart, and E.N. Lightfoot, *Transport Phenomena*, Chap. 8, Wiley, New York, 1960.
52. S. Hampshire, Engineering properties of nitrides, in *Ceramics and Glass: Engineered Materials Handbook*, Vol. 4, ASM International, Materials Park, OH, 1991, pp. 812–820.
53. W.J. Parker, R.J. Jenkins, C.P. Butler, and G.L. Abbot, Flash method of determining thermal diffusivity, heat capacity, and thermal conductivity, *J. Appl. Phy.* **32**(9), 1979–1984 (1961).
54. T. Log and T.B. Jackson, Simple and inexpensive flash technique for determining thermal diffusivity of ceramics, *J. Am. Ceram. Soc.* **74**(5), 941–944 (1991).

55. Peter T.B. Shaffer, Engineering Properties of Carbides, in *Ceramics and Glass: Engineered Materials Handbook*, Vol. 4, ASM International, Materials Park, OH, 1991, pp. 804–811.
56. D.W. Richerson, *Modern Ceramic Engineering*, Marcel Dekker, New York, 1992.
57. D.V Ragone, *Thermodynamics of Materials,* Vol. 1, Wiley, New York, 1995, p. 12.
58. H.M. Rosenberg, *The Solid State,* 2nd edn., Chap. 5, Oxford University Press, New York, 1978.
59. Thermochemical and Physical Property database, Version 2.2, ESM software.